ACS APPLIED MATERIALS & INTERFACES

Research Article

www.acsami.org

Hybrid Lipid-Capped Mesoporous Silica for Stimuli-Responsive Drug Release and Overcoming Multidrug Resistance

Ning Han,[†] Qinfu Zhao,[†] Long Wan,[†] Ying Wang,[†] Yikun Gao,[§] Pu Wang,[‡] Zhanyou Wang,[‡] Jinghai Zhang,[§] Tongying Jiang,[†] and Siling Wang*[,†]

[†]Department of Pharmaceutics, School of Pharmacy, Shenyang Pharmaceutical University, 103 Wenhua Road, Shenyang, Liaoning Province 110016, P. R. China

[‡]College of Life and Health Sciences, Northeastern University, Shenyang 110004, P. R. China

[§]School of Medical Devices, Shenyang Pharmaceutical University, Shenyang 110016, P. R. China

Supporting Information

ABSTRACT: Multidrug resistance (MDR) is known to be a great obstruction to successful chemotherapy, and considerable efforts have been devoted to reverse MDR including designing various functional drug delivery systems. In this study, hybrid lipid-capped mesoporous silica nanoparticles (LTMSNs), aimed toward achieving stimuli-responsive drug release to circumvent MDR, were specially designated for drug delivery. After modifying MSNs with hydrophobic chains through disulfide bond on the surface, lipid molecules composing polymer D-α-tocopherol polyethylene glycol 1000 succinate (TPGS) with molar ratio of 5:1 were subsequently added to self-assemble into a surrounded lipid layer via hydrophobic interaction acting as smart valves to block the pore channels of carrier. The obtained LTMSNs had a narrow size distribution of ca. 190 nm and can be stably dispersed in body fluids, which may ensure a long circulating time and ideal enhanced permeability and retention effect. Doxorubicin (DOX) was chosen as a model drug to be encapsulated into LTMSNs. Results showed that this hybrid lipid-capped mesoporous silica drug delivery system can achieve redox and pH-responsive release of DOX, thereby avoiding the premature leakage of drug before reaching the specific site and releasing DOX within the cancerous cells. Owing to the presence of TPGS-containing lipid layer, LTMSNs–DOX exhibited higher uptake efficiency, cytotoxicity, and increased intracellular accumulation in resistant MCF-7/Adr cells compared with DOX solution, proving to be a promising vehicle to realize intracellular drug release and inhibit drug efflux.

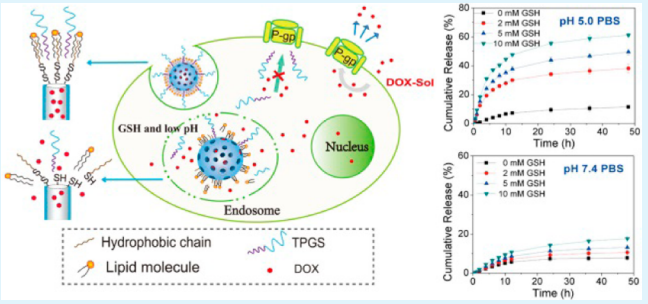

KEYWORDS: *mesoporous silica, lipid, polymer, drug delivery, stimuli-responsive release, multidrug resistance*

INTRODUCTION

It is well-known that the emergence of multidrug resistance (MDR) is a main obstacle for successful chemotherapy,[1] since many initially sensitive tumors will ultimately relapse to exhibit MDR phenotype and show resilience against structurally and mechanistically new drugs.[2] Generally, MDR is a complicated phenomenon that can be generated through multiple mechanisms,[3] and the primary cause is the increased drug efflux mediated by P-glycoprotein (P-gp), a member of adenosine 5′-triphosphate (ATP)-binding cassette (ABC) transporters, which can actively transport a broad range of anticancer drugs across the biological membranes.[4] Considerable efforts have been made to reverse MDR including coadministrating P-gp inhibitors;[5] unfortunately, the low efficiency and toxic side effects resulting from poor specificity have limited their applications in clinical trials. Therefore, more effective strategies should be exploited.

With the blossom of nanotechnology, smart drug delivery systems (DDSs) show great prospects for circumventing MDR.[6] An ideal DDS should promote the intracellular accumulation of drug in the targeted cells and maintain drug concentration in an optimum level to take effect. As one of the most excellent representatives, a stimuli-responsive DDS with the ability of controlling drug release spatially and temporally could avoid leakage of drug during circulation and achieve storm release at the targeting site thus eliminating the toxic effects caused by lack of selectivity and improving the intracellular accumulation of drugs sufficiently to reach the therapeutic level.[7] Recently, stimuli-responsive DDSs based on mesoporous silica nanoparticles (MSNs) have drawn much attention due to the unique properties of MSNs.[8] The extremely large surface area and pore volume of MSNs could accommodate drug molecules within the pore channels with a high payload,[9] and the easily modified surface could facilitate the attachment of different kinds of "gatekeeper" on the outlets of pore to control the release of drug. Various gatekeepers

Received: November 25, 2014
Accepted: January 13, 2015
Published: January 13, 2015

DOI: 10.1021/am5082793
ACS Appl. Mater. Interfaces 2015, 7, 3342–3351

including inorganic CdS and Fe_3O_4 nanoparticles, cyclodextrin, polymers, and biomacromolecules were cultivated as "caps" to block/unblock the entrance of pore, and stimuli such as pH, temperature, redox, light, and enzyme could trigger the release of incorporated drug.[10−14] The achievements of such DDSs were remarkable, premature leakage of drug was greatly suppressed, and nearly all the drug molecules were programmed to release within the tumor cells. However, after the drug molecules were released into the cytoplasm, exposure to the efflux pump again became inevitable,[15] and how to prevent the drugs from subsequent extrusion by P-gp still remains a challenge.

Herein, we introduced the hybrid lipid-capped mesoporous silica nanoparticles (LTMSN) to address the above problem and improve the antitumor efficacy against MDR cancerous cells. MSNs with diameter of 100 nm were fabricated and then capped with a disulfide bond-linked, D-α-tocopherol polyethylene glycol 1000 succinate (TPGS 20% mol)-containing lipid layer. It was reported that the glutathione (GSH) concentration within several intracellular compartments (usually 2−10 mM) was 100−1000 times higher than that in the extracellular environment (~2−20 μM).[16] And the endocellular GSH concentration in most cancerous cells was at least 3-fold higher than that in normal cells,[17] which means that the hybrid lipid layer can act as "pore blocker" during circulation since the disulfide bond was steady in the extracellular fluids. When the carriers were transported into cells, especially the tumor cells, the disulfide bond can be rapidly cleaved by high concentration of GSH leading to the detachment of lipid layer and "on demand" release of drug. Adopting the hybrid lipid layer as the gatekeeper has many other advantages including facilitating the cellular uptake of carrier due to the high affinity of the lipid layer with cell membrane,[18] an inherent nature lecithin possessed, improving the dispersing stability of MSN in saline buffer,[19,20] and the overall bioavailability of the carrier.[21] In particular, the TPGS inserted in the lipid layer was reported to have the ability of inhibiting drug efflux by suppressing the activity of P-gp ATPase without affecting the membrane fluidity, of which the specific mechanism was that TPGS could inhibit the hydrolysis of ATP by ATPase via binding to the ATPase-substrate complex, but TPGS does not directly compete with the substrate. Since the efflux function of P-gp was ATP-dependent, TPGS, which proved to be an uncompetitive inhibitor of P-gp ATPase, could block the energy supply for the pumping out of drug, thereby helped to retain drugs within cells for overcoming MDR.[22] TPGS was also able to induce the apoptosis of tumor cell acting as an anticancer agent and exhibited a synergistic effect with many anticancer drugs.[23] Moreover the polyethylene glycol (PEG) chains in the structure can prolong the systemic circulation time in the bloodstream after intravenous injection, which allows better accumulation of drug carriers in the tumor site by enhanced permeability and retention (EPR) effect.[21]

Doxorubixin (DOX) is one of the most potent anticancer drugs applied in clinic; it can treat various human malignancies by intercalation into the DNA double helix to induce DNA damage.[24] However, the toxicity resulting from nonspecific action appeared to be a serious side effect of DOX-based therapy.[25] And it is essential to release and deliver DOX in cytoplasm and directly into the nucleus of cancerous cells. Moreover, it was also a substrate of P-gp, which was ready to be pumped out after cell internalization, which is the primary cause of drug resistance and regeneration of tumor.[26] The aim of our research was to establish a stimuli-responsive intracellular delivery system concomitant with the ability to overcome drug resistance, which may lead to enhanced cancer chemotherapy. To investigate whether LTMSNs possessed the features mentioned above, DOX was selected as a model drug to be encapsulated within LTMSNs and delivered to DOX-resistant human breast cancer MCF-7/Adr cell line. The in vitro drug release behavior, cytotoxicity, cellular uptake efficiency, and inhibition of P-gp were systematically investigated to evaluate the effectiveness of MDR reversion after the administration of LTMSNs−DOX (see Scheme 1).

Scheme 1. Schematic Representation of DOX-Loaded LTMSNs for pH/Redox-Triggered DOX Release and Inhibition of P-gp-Mediated Drug Efflux

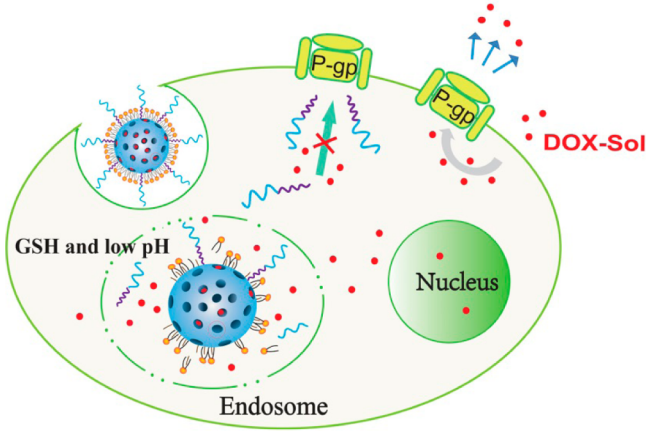

1. MATERIALS AND METHODS

Tetraethyl orthosilicate (TEOS, 98%), triethanolamine (TEA), and hexadecyl trimethylammonium chloride (CTAC, >99%) were obtained from Tianjin Bodi Chemical Holding Co., Ltd. (Tianjin, China). 3-mercaptopropyltrimethoxysilane (MPTMS), 2,2′-dipyridyl disulfide, octadecanethiol, glutathione (GSH), and D-α-tocopherol polyethylene glycol 1000 succinate (TPGS) were purchased from Aladdin Chemistry Co., Ltd. (Shanghai, China). Soybean lecithin was from LIPOID GmbH (Ludwigshafen, Germany). Anticancer drug doxorubicin hydrochloride (DOX) was kindly provided by Zhejiang Hisun Pharmaceutical Co., Ltd. (Zhejiang, China). Cell culture medium RPMI 1640, fetal bovine serum (FBS), trypsin-EDTA solution (0.25% trypsinwith 0.53 mM EDTA), and penicillin-streptomycin were obtained from GIBCO, Invitrogen Co., Ltd. (Carlsbad, U.S.A.). 3-(4,5-Dimethylthiazol-2-yl)-2,5-diphenyl tetrazolium bromide (MTT) was supplied by Amreso (U.S.A.). Fluorescent Hoechst 33258 was obtained from Molecular Probes Inc. (Eugene, OR, U.S.A.). All other chemicals were of analytical grade and used without further purification.

1.1. Cell Culture. The cell lines MCF-7 and MCF-7/Adr used in this study were obtained from American Type Culture Collection (ATCC, Manassas, VA) and were cultured in RPMI 1640 medium with 10% fetal bovine serum (FBS) and 100 units/mL penicillin G sodium and 100 μg/mL strepto-mycin sulfate at 37 °C in a humidified atmosphere with 5% CO_2.

2. PREPARATION AND CHARACTERIZATION

2.1. Preparation of Hybrid Lipid-Capped Mesoporous Silica Nanoparticles (LTMSNs). *2.1.1. Synthesis of MSNs−SH.* Mesoporous silica nanoparticles were synthesized according to the procedure from literature.[27] Briefly, CTAC (1.25 g), TEA (2.0 mL), and ethanol (5.0 mL) were dissolved in 40 mL of deionized water. TEOS (2.90 mL) was then introduced dropwise to the above solution

DOI: 10.1021/am5082793
ACS Appl. Mater. Interfaces 2015, 7, 3342−3351

with intensive stirring, and the mixture was maintained at 60 °C for 2 h. The obtained white precipitate was collected by centrifugation at 13 000 rpm and washed with ethanol three times. Then post-graft method was used for the introduction of thiol group. It was conducted by redispersing the synthesized nanoparticles in absolute ethanol containing MPTMS (0.40 mL) and refluxing at 77 °C for 6 h. For template extraction, NH_4NO_3 (1.0 g) was subsequently added and stirred overnight at 80 °C to remove the surfactant; the final product was centrifuged and stored in ethanol.

2.1.2. Synthesis of MSNs−S−S−C_{18}. The surfactant-free MSNs−SH was then treated with ethanol solution of 2,2′-dipyridyl disulfide at room temperature for 24 h under vigorous stirring to undergo the disulfide bond exchange reaction. The resulting precipitate was centrifuged and washed with excess ethanol to yield pyridyl−disulfide MSNs (Py−S−S−MSNs). To obtain MSNs−S−S−C_{18}, Py−S−S−MSNs were further allowed to react with the hydrophobic chain octadecanethiol at 40 °C for another 48 h. And the final particles were isolated by centrifugation and dried overnight at room temperature in vacuum.

2.1.3. Preparation of Hybrid Lipid-Capped Mesoporous Silica Nanoparticals (LTMSNs). Hybrid lipid-capped mesoporous silica nanoparticals were prepared using a modified thin-film hydration method. Hydrophobic MSNs−S−S−C_{18} (20 mg) was placed in a glass vial with 2 mL of chloroform and sonicated for 5 min to form good dispersion, and then a solution of previously dissolved soybean lecithin (5 mg) and TPGS with molar ratio of 5:1 was added to the suspension. The solvent was evaporated under reduced pressure to let lipid and TPGS molecules self-assemble into a lipid layer on the surface of MSNs−S−S−C_{18} via hydrophobic interaction. The resulting lipid film was resuspended in pH 7.4 phosphate-buffered saline (PBS, 2 mL) and sonicated for 2 min. Repeated centrifugation was conducted to remove the excess phospholipid, and the obtained LTMSNs were used for further experiment. And the sample named LMSNs, which was prepared in the same way but capped with a lipid layer without TPGS, was used as one of the control groups in the following experiments.

2.2. Drug Loading and Encapsulation Efficiency. Prior to lipid capping, MSNs−S−S−C_{18} (20 mg) was incubated with 2 mL of a methanol solution of DOX (2 mg/mL) for 24 h at room temperature with intermittent stirring for full absorption of drug. After centrifugation at 10 000 rpm, the DOX-loaded MSNs were isolated and dried under vacuum. Then 23 mg of the DOX-loaded particles was redispersed in chloroform, and lipid capping was conducted following the procedure of Section 2.1.3 described above. The drug loading efficiency (LE%) was ascertained according to the following formula. The weight of encapsulated DOX was obtained by subtracting the unabsorbed drug in the supernatant and those losses during the lipid capping process from the initial amount of DOX added.

$$\text{LE\%} = \frac{\text{weight of encapsulated DOX}}{\text{weight of DOX-loaded LTMSNs}} \times 100$$

2.3. Characterization of the Nanoparticles. The material structure of MSNs and LTMSNs were observed by field-emission transmission electron microscopy (TEM) and scanning electron microscopy (SEM). For TEM imaging, nanoparticles were dispersed in deionized water and dropped on the carbon-coated copper grid. To visualize the presence of lipid layer on MSNs, LTMSNs were treated with 2% (w/w) solution of uranyl acetate for 1 min for negative staining. After air drying, samples were imaged using FEI Tecnai G2 F30 (Netherlands), operated at an acceleration voltage of 200 kV. For SEM imaging, the desiccative nanoparticles were sprayed with gold on a carbon grid and were imaged using Zeiss Supra 35 (Germany).

The particle size distributions and zeta potentials of the MSNs and LTMSNs were examined using Zetasizer Nano (Malvern Instruments Ltd., United Kingdom), and the nitrogen adsorption/desorption analysis was performed using an adsorption analyzer (V-Sorb 2800P, China). According to the adsorption data, the Brunauer−Emmett−Teller (BET) and Barrett−Joyner−Halenda (BJH) models were used to calculate the specific surface areas and the pore size of the carriers, respectively. Thermogravimetric analysis (TGA) was also conducted using the TGA-50 instrument (Shimadzu, Japan) to investigate the weight loss after each step of functionalization with a heating rate of 5 °C/min under a nitrogen flow. Fourier-transform infrared spectrophotometry (FT-IR) spectra with a range from 400 to 4000 cm^{-1} were recorded on an FT-IR spectrometer (Bruker IFS 55, Switzerland) by compressing the samples into pellets with KBr.

2.4. In Vitro Stimuli-Responsive Drug Release. To prove the stimuli-responsive release feature, DOX release from LTMSNs was performed in PBS with different pH values (pH 7.4 and 5.0) and GSH concentrations (0, 2, 5, and 10 mM). LTMSNs−DOX (3 mL, 10 mg/mL) was transferred into a dialysis bag (MWCO 14 000 Da) and then was submerged into 30 mL of PBS at 37 °C with continuous shaking at the speed of 100 rpm. Release medium of 1 mL was withdrawn at predetermined time intervals, and fresh medium with equal volume was used to replenish the solution. The concentration of released DOX was determined via measuring the absorbance of DOX at 480 nm by UV−vis spectrophotometer (UV-2000, UNICO, U.S.A.), and the cumulative release percentage of DOX was calculated according to the following formula. The results were averaged after three measurements.

$$\text{release percentage}(\%) = \frac{\text{amount of DOX released}}{\text{amount of DOX encapsulated in LTMSNs}} \times 100$$

2.5. Cellular Uptake. The quantitative cellular uptake of DOX from DOX−Sol, MSNs, LMSNs, and LTMSNs was investigated by fluorescence-activated cell sorter (FACS). MCF-7 and MCF-7/Adr cells were seeded in six-well plates at a density of 5×10^5 per well and incubated overnight. After they were rinsed with PBS, the cells were treated with DOX−Sol, MSNs−DOX, LMSNs−DOX, and LTMSNs−DOX in serum-free RPMI 1640 medium for 1, 2, and 4 h at 37 °C. The concentration of DOX was 5 μg/mL. At the end of the experiment, cells within each well were trypsinized, washed with cold PBS three times, and resuspended in 400 μL of PBS. The mean fluorescence intensity (MFI) was measured by FACS (FACS Calibur, Becton Dickinson, U.S.A.) and blanked with untreated cells.

For microscopic observation, MCF-7 and MCF-7/Adr cells were seeded onto round glass coverslips in 24-well plates. After 12 h of attachment, the medium was replaced with fresh serum-free RPMI 1640 medium containing DOX−Sol, MSNs−DOX, LMSNs−DOX and LTMSNs−DOX with equivalent DOX concentration of 5 μg/mL. After 4 h of incubation, the cells were washed with cold PBS three times and fixed with 4% formaldehyde. The nuclei were then counterstained by Hoechst 33258 for 20 min. Observation of the fixed cells was conducted using a Leica DM-6000 CS microscope (Leica Instruments Inc., Wetzlar, Germany).

To examine the efflux of DOX, MCF-7/Adr cells were first incubated with DOX−Sol, MSNs−DOX, LMSNs−DOX, and LTMSNs−DOX (DOX concentration of 5 μg/mL) for 4 h. After triply rinsing the PBS to remove the nanoparticles that had adhered to the cell surface, cells were further allowed to incubate with fresh medium for 1, 2, and 4 h at 37 °C. Finally, cells were collected for fluorescence intensity analysis by FACS or fixed for observation with confocal laser scanning microscopy to determine the accumulation of DOX within the cells.

2.6. Cell Viability. The in vitro cytotoxicity of blank nanoparticles and DOX−loaded samples toward MCF-7 and MCF-7/Adr cells was evaluated by MTT assay. Briefly, cells were seeded onto 96-well plates at a density of 2.0×10^4 cells/well. After 24 h of attachment, the culture medium was removed, and cells were incubated with serum-free medium containing DOX−Sol, MSNs−DOX, LMSNs−DOX, and LTMSNs−DOX at serial DOX concentrations of 0.01, 0.1, 1, 10, and 100 μg/mL for MCF-7 and MCF-7/Adr cells. At predetermined time intervals, 50 μL of MTT solution (2 mg/mL) was added to the culture medium and incubated for additional 4 h to quantify cell viability. After the removal of supernatant, 150 μL of dimethyl sulfoxide was added to each well, and the 96-well plates were agitated for 10 min to fully dissolve the produced formazan crystals. Finally, the absorbance at

DOI: 10.1021/am5082793
ACS Appl. Mater. Interfaces 2015, 7, 3342−3351

Scheme 2. Preparation Process of DOX-Loaded LTMSNs and Detailed Mechanism of Stimuli-Responsive Drug Release

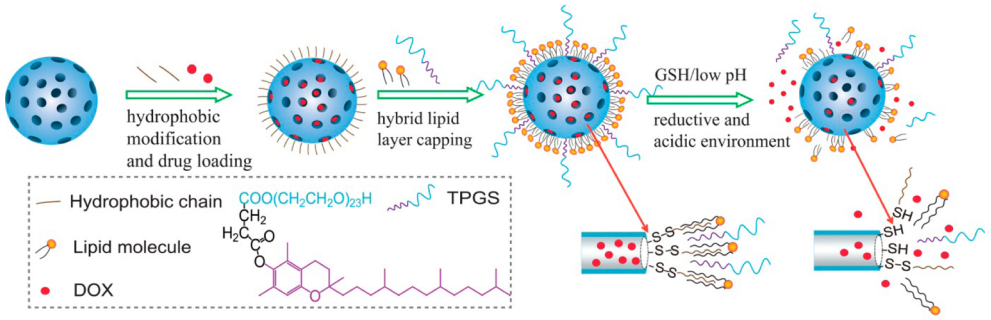

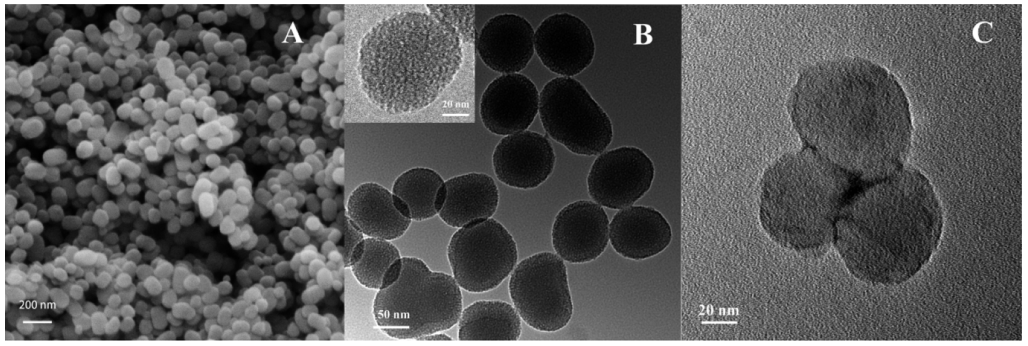

Figure 1. SEM (A) and TEM (B) images of MSNs; TEM image of LTMSNs (C) stained by uranyl acetate.

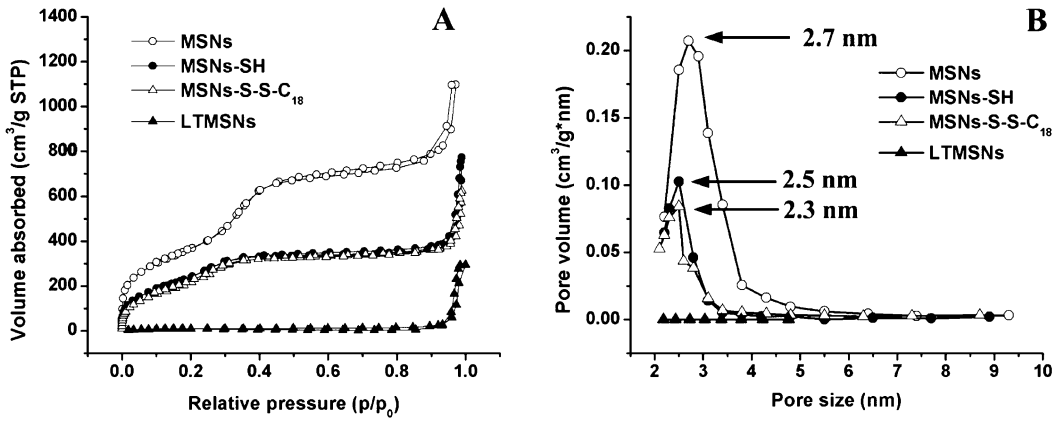

Figure 2. Nitrogen adsorption−desorption isotherms (A) and pore diameter distribution (B) of MSNs, MSNs−SH, MSNs−S−S−C_{18}, and LTMSNs.

wavelength of 570 nm was measured using an iMark microplate reader (Bio-RAD, CA, U.S.A.). Cells without treatment were used as control.

3. RESULTS AND DISCUSSION

3.1. Preparation and Characterization of LTMSNs. The hybrid lipid-capped mesoporous silica nanoparticles (LTMSNs) with a TPGS-containing lipid layer as smart cap were prepared through a sequential modification on the MSNs as described in Scheme.2.

MSNs of ca. 100 nm were synthesized via adjusting the amount of TEA added in the preparation process, and the reason for the selection of MSNs with ca.100 nm was that nanoparticles with diameter between 100 and 200 nm were reported to have the strongest EPR effect.[28] MSNs were then modified with thiol group before template extraction via the post-graft method, which can control the position of functionalization.[29] After the formation of CTAC micelle containing MSNs, MPTMS was added to react with the saline group of SiO_2. Since the pore channels were occupied by the micelle template, the MPTMS cannot penetrate into the pore to contact with the internal surface; thus, most thiol groups exist on the external surface of MSNs, which effectively prevented the "pore-blocking" effect caused by the addition of organosilane. The MSNs−SH were then treated with 2,2′-dipyridyl disulfide to obtain Py−S−S−MSNs with cleavable disulfide bonds. Subsequently, octadecanethiol was covalently grafted onto MSNs to form a densely packed hydrophobic shell by disulfide bond exchange reaction. Lipid and TPGS molecules with molar ratio of 5:1 were added to self-assemble into a lipid layer acting as caps around MSNs.

The synthesized spherical MSNs were uniformly sized and had an average diameter of ca. 100 nm as shown in the SEM image (Figure 1A). And the three-dimensional wormhole pore arrangement of MSNs can be clearly seen in the TEM image

DOI: 10.1021/am5082793
ACS Appl. Mater. Interfaces 2015, 7, 3342−3351

(Figure 1B). For LTMSNs, the surfaces became rough, and the dark ring surrounding MSNs in Figure 1C proved the presence of lipid layer stained by uranyl acetate via the ionic interactions with phospholipids.[19]

The adsorption−desorption isotherm curves and pore size distributions of MSNs, MSNs−SH, MSNs−S−S−C_{18}, and LTMSNs are shown in Figure 2. Parameters including BET surface area (S_{BET}), cumulative pore volume (V_p), and BJH average pore size (W_{BJH}) are listed in Table 1.Though MSNs suffered notable decrease in surface area and pore volume, and shrinkage of pore size from 2.7 to 2.3 nm after serial functionalization process, the pore channels were still available to encapsulate drug with high efficiency and allow drug molecules to diffuse freely. However, after capping MSNs with hybrid lipid layer, the surface area decreased sharply to 31 m^2/g, and the pores became undetectable, which indicated that the pores were completely blocked. Therefore, drug loading was performed before the lipid capping process.

Table 1. Nitrogen Adsorption−Desorption Analysis of Various MSNs

sample	S_{BET} (m^2/g)	V_p (cm^3/g)	W_{BJH} (nm)
MSNs	1371	0.93	2.7
MSNs−SH	967	0.69	2.5
MSNs−S−S−C_{18}	716	0.472	2.3
LTMSNs	31	0	<2

The FT-IR spectra of MSNs with different functionalization were compared in Figure 3; the absorption peak appeared at ~2560 cm^{-1}confirmed the presence of thiol group on MSNs. After reaction with octadecanethiol, the absorption peak of thiol group disappeared due to the formation of disulfide bond. And the strengthened absorbance at 2800−3000 cm^{-1} assigned to C−H stretching suggested the successful grafting of octadecanethiol. The absorption peak appeared at 1231 and 1738 cm^{-1} that belongs to P═O and C═O demonstrated the presence of hybrid lipid layer on MSNs. Consistent with phenomenon observed in Figure 3, the MSNs−S−S−C_{18} with hydrophobic surface property could only suspended in $CHCl_3$,whereas the MSNs could be well-dispersed in water.

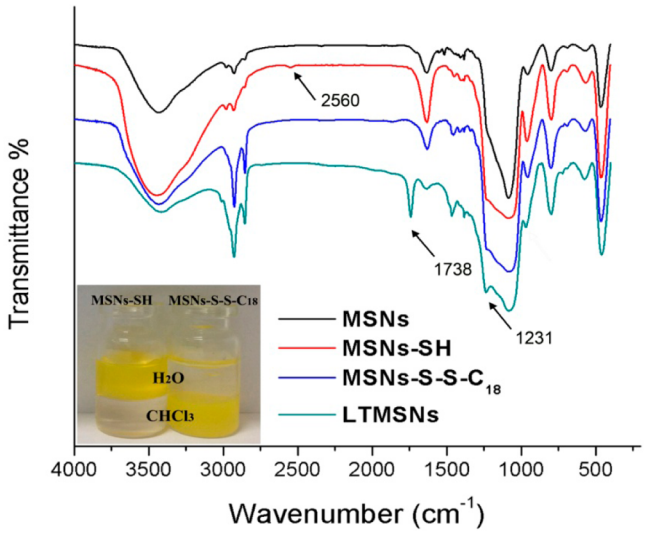

Figure 3. FT-IR spectra of MSNs, MSNs−SH, MSNs−S−S−C_{18}, and LTMSNs. (inset) Photograph of the distribution of FITC-labled MSNs and MSNs−S−S−C_{18} in water and $CHCl_3$.

The data of zeta potential measurement (Figure 4) could also confirm the above result. The MSNs−SH had a zeta potential value of −30 mV but increased to ~0 mV after lipid capping owing to the shield effect of the neutrally charged lipid layer and PEG chains of TPGS. The hydrodynamic diameter of MSNs was ca.123 nm, as shown in Figure 4, a little larger than what was observed in TEM image due to the hydrated layer in aqueous environment.[27] As for LTMSNs, the hydrodynamic diameter grew to 196 nm, which further demonstrated the presence of lipid layer on the outermost surface of MSNs. And it is worth mentioning that the charge-stabilized property of MSNs via the ionization of hydroxyl groups on the surface posed limitation to their bioapplication. MSNs can be easily destabilized and tend to aggregate in the saline buffer, and the aggregation will accelerate after the absorption of proteins in the serum leading to the rapid clearance by reticuloendothelial system (RES),[30] which is extremely undesired for intravenous administration, a frequent route for drug delivery. After capping the MSNs with the TPGS-containing lipid layer, the silanol groups were shielded, and nanoparticles can be stably dispersed in PBS and saline containing 5% BSA (physiological concentration of BSA). The hydrodynamic diameter remained the same compared with that in water (Supporting Information), which indicates that the TPGS-containing lipid layer can improve the dispersing stability of MSNs and provide the prerequisite for the safe administration of nanoparticles intravenously. The PEG chains of TPGS can help to avoid the recognition and capture by RES and prolong the circulation time to facilitate the accumulation of drug-loaded carriers at the tumor site by the EPR effect.[31]

The TGA curves of various samples are shown in Figure 5. Within the temperature range from 50 to 150 °C, weight loss of ~13% was observed for MSNs−SH, which should be attributed to thiol group on the surface. As for MSN−S−S−C_{18}, an additional weight loss of ~10% could be ascribed to the hydrophobic chains grafted on MSNs. And the weight loss of LMSNs and LTMSNs reached as high as 41.8% and 45.2%, respectively. The above results proved the successful functionalizatin of MSNs after each step.

3.2. Drug Loading Efficiency and Stimuli-Responsive Drug Release. Drug loading was executed after the grafting of hydrophobic chains and thus was conducted in the organic solvent of methanol. Since the pore volumes and pore sizes of MSNs−S−S−C_{18} were greatly preserved, MSNs−S−S−C_{18} can carry DOX as much as 16% by physical absorption. While the loading efficiency inevitably reduced to 11.5% after the lipid capping process in which the loss of DOX was minimal, it was the extra weight contributed by the added lipid and TPGS that should be responsible for the declined LE% in the calculation. To examine the detachment of lipid layer from MSNs and release of drug in a controlled manner, the DOX-encapsulated LTMSNs were exposed to PBS of pH 7.4 and 5.0 under various GSH concentrations. The release profiles are shown in Figure 6. In the absence of GSH, the cumulative release of DOX from LTMSNs were quite slow, only 6% and 8% at pH 7.4 and 5.0 within the period of 48 h, suggesting that a prominent capping efficiency can be achieved by the hybrid lipid layer regardless of the pH value, and the premature leakage of drug can be greatly eliminated in the normal physiological environment. In contrast, accelerated release of DOX can be detected after the addition of GSH due to the removal of hybrid lipid layer

DOI: 10.1021/am5082793
ACS Appl. Mater. Interfaces 2015, 7, 3342−3351

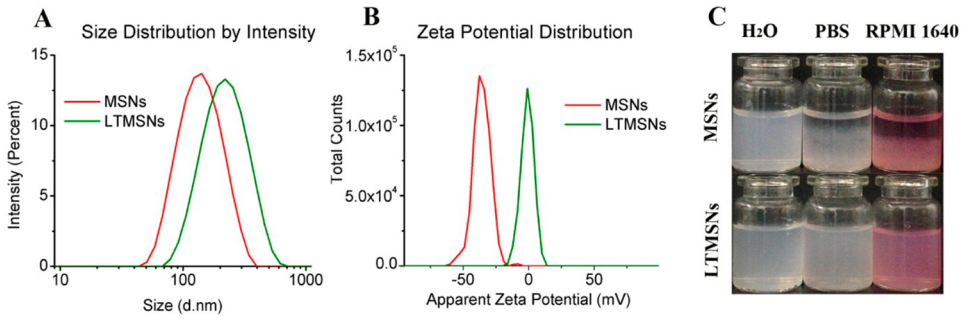

Figure 4. Size distribution (A), zeta potential (B), and dispersing stability (C) of MSNs and LTMSNs.

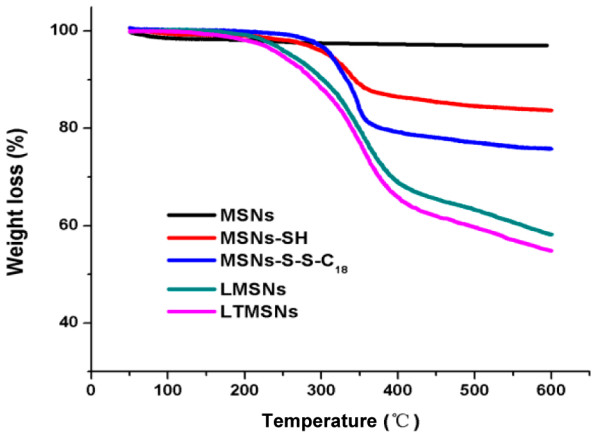

Figure 5. TGA curves of MSNs, MSN−SH, MSN−S−S−C_{18}, LMSNs, and LTMSNs.

capping, the release rate, and extent elevated with the increasing of the GSH concentration. The amount of released DOX can reach as high as 17.6% at pH 7.4 and 60% at pH 5.0 under 10 mM GSH, which confirmed the pH and reduction dual-responsive release of DOX from LTMSNs. The obtained results demonstrated that the release of DOX was dominated by two factors, the dissociation of lipid layer and electrostatic interaction between MSNs and DOX. Because of the cleavage of the disulfide bond in the simulated intracellular reducing conditions, the lipid layer will detach from the surface of the carrier leaving the pore unblocked, which favors the out diffusion of drug. And the reason for the differed release rate and extent of DOX under various GSH concentrations was that under low GSH concentration, a certain percentage of the DOX molecules was still entrapped in the pores of MSNs due to the incomplete removal of the hybrid lipid layer. At high GSH concentrations, the lipid layer dissociated thoroughly leading to the full opening of pores and rapid release of DOX. However, after the reopening of pores, the significantly diversified cumulative release of DOX under different pH condition can be explained as that at pH value of 7.4, the DOX molecules were tightly entangled within the pore due to the electrostatic attraction with MSNs, and when the pH value declined to 5.0, similar to the acidic condition at the tumor site, the protonation of silanol groups weakened the electrostatic interactions,[32,33] thus leading to the gradual release of DOX.

3.3. Cell Internalization and Intracellular Release. To examine the intracellular release of drug, the red fluorescence of DOX within sensitive MCF-7 and resistant MCF-7/Adr cells was quantified and compared by FACS and CLSM after incubation with various DOX formulations for different periods of time. The results are shown in Figure 7. Regarding MCF-7, the fluorescence intensity in cells treated with MSNs−DOX was significantly higher than that incubated with DOX−Sol for the same period of time. DOX−Sol can enter the cells only by diffusion, while DOX within the MSNs can be effectively uptaken by cells via the carrier-mediated endocytosis.[15] After the capping of lipid layer, the highest fluorescence intensity was observed for LMSNs due to the favorable affinity between lecithin and cell membrane, which can dramatically promote the internalization of DOX-loaded carrier.[34] However, the uptake efficiency slightly lowered when inserting TPGS into the lipid layer, since the steric hindrance provided by PEG aqueous layer might impede the full contact of the carrier with the

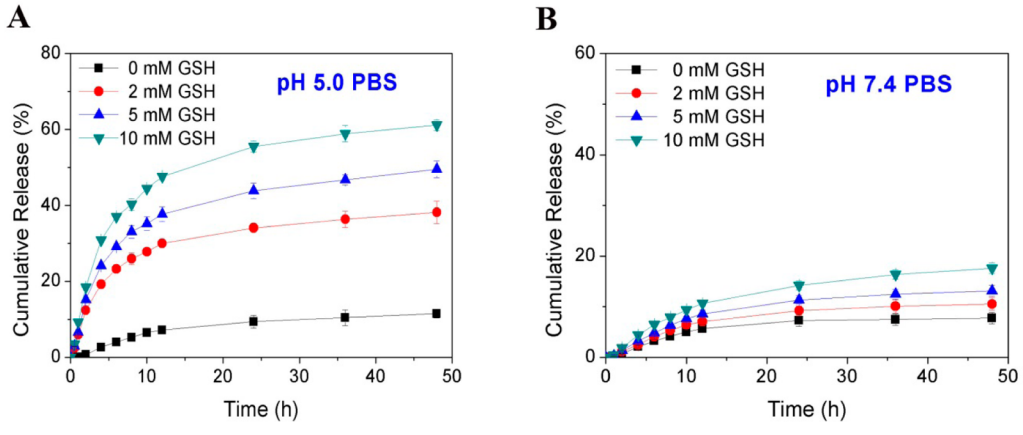

Figure 6. Cumulative release profiles of LTMSNs−DOX in pH 5.0 PBS (A) and pH 7.4 PBS (B) under different GSH concentrations.

DOI: 10.1021/am5082793
ACS Appl. Mater. Interfaces 2015, 7, 3342−3351

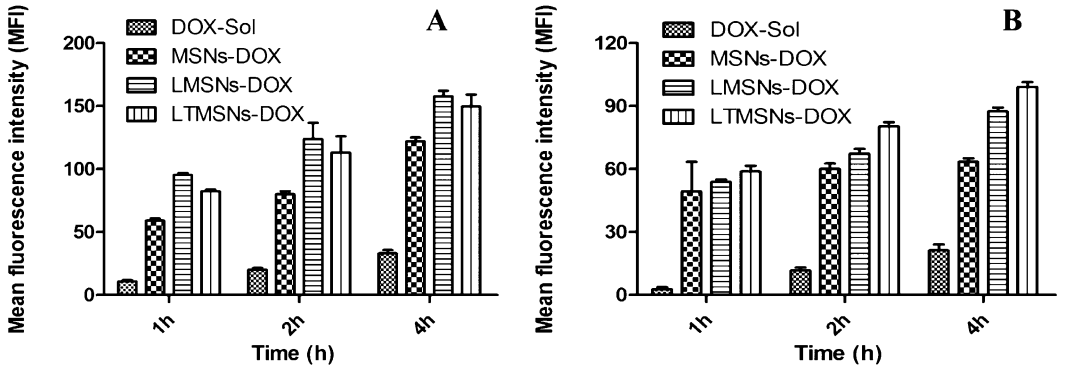

Figure 7. MFI of DOX−Sol, MSNs−DOX, LMSNs−DOX, and LTMSNs−DOX in MCF-7 (A) and MCF-7/Adr cells (B).

cells.[35] For all the groups, the intracellular concentration of DOX increased with the extension of incubation time within 4 h. In the case of MCF-7/Adr cells, the fluorescence intensity of DOX−Sol group was nearly 3 times lower than that in MCF-7 cells, demonstrating the drug efflux effect of P-gp. The cellular uptake of DOX within MSNs markedly augmented, since MSNs could bypass P-gp-mediated efflux through the endocytosis pathway and the process was ATP-consuming, which consequently could counteract the activity of P-gp to some degree.[15] And the accumulation of LMSNs−DOX was much higher compared with that of MSNs, similar to the trend observed for MCF-7. The reasons accounting for this phenomenon are as follows. For one thing, the cell membrane is known to carry an overall negative charge; therefore, the negatively charged MSNs must overcome an electrostatic barrier to reach its surface, while the almost neutrally charged LMSNs can exhibit stronger adhesion ability and higher internalization rate than MSNs due to the structural similarity with cell membrane. For another, MSNs may suffer certain loss of the incorporated DOX due to the premature leakage during incubation. When it came to LMSNs, capping with the lipid layer can greatly minimize the burst release of drug in the culture medium and achieve intracellular storm release resulting in the intenser fluorescence signal. And it is worthwhile to mention that MCF-7/Adr cells with strongest fluorescence signal was found to be the group treated with LTMSNs, which is quite different from that of MCF-7.The reason is that during the internalization process of LMSNs−DOX, part of the released DOX was pumped out by P-gp, yet the introduction of TPGS in LTMSNs could inhibit the efflux pump, which contributed to the better retaining of drug in cytoplasm.

In addition to FACS, confocal microscopy (CLSM) was employed to visualize the internalization and localization of DOX in cells. As for MCF-7 cells with low P-gp expression (Figure 8), free DOX could penetrate into cells with the prolonging of time and eventually arrive at the nucleus, while the red fluorescence became more pronounced when encapsulating DOX into MSNs and exhibited further enhancement after capping of TPGS-containing lipid layer. The strongest intensity was observed for LMSNs, which coincides well with the results of FACS. As expected, in the resistant MCF-7/Adr cells (Figure 9), the sign of Free DOX was too weak to be detected even after 4 h of incubation, due to the secretion of P-gp. After being incorporated into MSNs, the uptake of DOX notably increased but still was not as much as that of LMSNs. And the topmost accumulation of DOX was observed within MCF-7/Adr after exposure to LTMSNs, as indicated by the appearance of highest red fluorescence

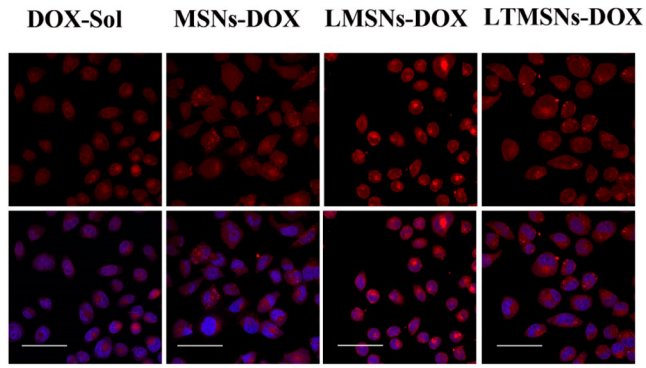

Figure 8. Confocal microscopy images of MCF-7 cells after treatment with various DOX formulations for 4 h. Scale bar represents 50 μm.

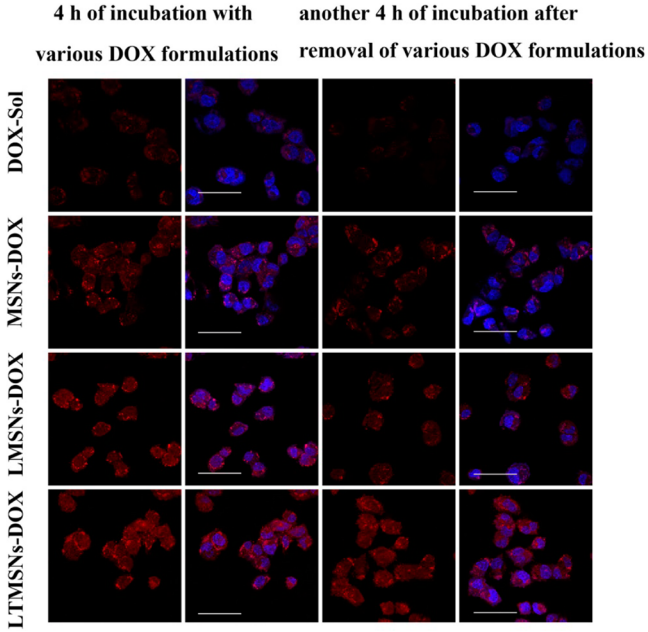

Figure 9. Internalization and retaining of DOX in MCF-7/Adr cells after treatment with various DOX formulations for 4 h and another 4 h of incubation after the removal of DOX formulations measured by confocal microscopy. Scale bar represents 50 μm.

intensity. It was intriguing to note that the wide distribution within cytoplasm and nucleic accumulation of DOX can be observed for group of LMSNs and LTMSNs, illustrating that the lipid cap can be rapidly cleaved upon entering the cells and that drugs can diffuse into the nucleus gradually.

DOI: 10.1021/am5082793
ACS Appl. Mater. Interfaces 2015, 7, 3342−3351

3.4. Inhibition of Drug Efflux. To monitor the inhibition effect of drug efflux, MCF-7/Adr cells were first cultured with the DOX formulations for 4 h.Then the DOX-containing medium was removed and replaced with fresh medium to allow further incubation for different times. The retaining of DOX within cells was quantified by FCM and CLSM. According to the results shown in Figure 10, the amount of free DOX

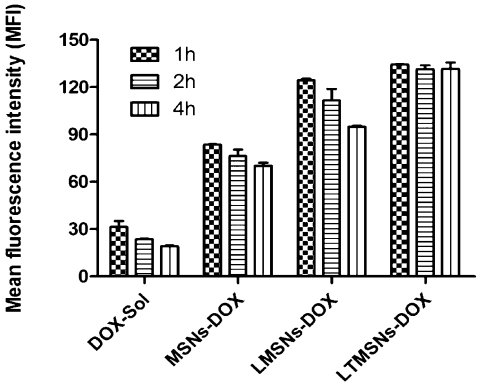

Figure 10. Efflux of DOX from various formulations by MCF-7/ADR cells at predetermined times of 1, 2, and 4 h.

uptaken by cells was extremely low, and gradually decreased with the passage of time as a result of P-gp efflux. The content of MSNs−DOX was much higher at the beginning but still underwent a time-dependent decline in the continuous period of incubation. A similar trend was observed for LMSNs−DOX as well, regardless of the significantly elevated accumulation of drug right after the internalization process. However, the strongest DOX intensity was observed when treating the MCF-7/Adr cells with LTMSNs−DOX, and there was no obvious decrease in fluorescence intensity within the time range of efflux experiment, which implies that the P-gp-mediated DOX efflux could be effectively reduced due to the presence of TPGS-containing lipid layer. The following images of CLSM in Figure 9 proved to be highly supportive of the obtained results above. Therefore, the improvement of uptake efficiency alone cannot guarantee the sufficient retaining of drug; only after combination with the subsequent inhibition of drug efflux, could the MDR be eventually overcame.

3.5. In Vitro Cell Viability. The cytotoxicity of various DOX formulations at different DOX concentrations and the corresponding amount of blank nanocarriers toward cell lines of MCF-7 and MCF-7/Adr were investigated by MTT essay, and the results are shown in Figure 11. The IC_{50} (concentration of test samples that can inhibit cell growth by 50%) was calculated using SPSS software 13.0 (SPSS Inc., Chicago, IL, U.S.A.), and the results are listed in Table 2. As for various

Table 2. IC_{50} Values of Different DOX Formulations against MCF-7 and MCF-7/Adr Cells

	IC_{50} (μg/mL)	
formulation	MCF-7	MCF-7/Adr
DOX−Sol	0.59	183.67
MSNs−DOX	0.30	122.04
LMSNs−DOX	0.32	58.46
LTMSNs−DOX	0.22	12.31

DOX formulations, the cytotoxicity was concentration- and time-dependent for both types of cells. In MCF-7/Adr cells with a high overexpression of P-gp, the IC_{50} of DOX−Sol was 183 μg/mL, 310 times higher that of MCF-7 cells with IC_{50} of 0.59 μg/mL, demonstrating a strong efflux effect. Once loading the DOX into MSNs, the cytotoxicity greatly increased due to the facilitated cellular uptake of DOX and bypass of P-gp via the endocytic pathway. After the capping of lipid layer, the cytotoxic effect of LMSNs−DOX further increased 2-fold as a result of enhanced internalization and storm release of drug in the cytoplasm, while the strongest cytotoxicity was obtained for LTMSNs−DOX, since, departing from the promoted accumulation of DOX, the presence of TPGS could prevent the expelling of drug by efflux pump and exhibit collaborative antitumor effect (Supporting Information). It was reported that TPGS could selectively induce the generation of reactive oxygen species (ROS) and apoptosis of cancer cells but cause almost no harm to normal cells, which are resistant to oxidative stress.[23] And the IC_{50} of LTMSNs−DOX, LMSNs−DOX, and MSNs−DOX was 15-, 3-, and 1.5-fold lower than that of DOX−Sol, respectively. According to the results, LTMSNs demonstrated the ability to overcome MDR. As for MCF-7 cells, a parallel trend on proliferative inhibition was found when the concentration of DOX was lower than 1 μg/mL, for the same reason as has been discussed above. The variation between groups became negligible with the continuous increasing of DOX concentration, since all the DOX formulations can enter the cells easily and be retained within

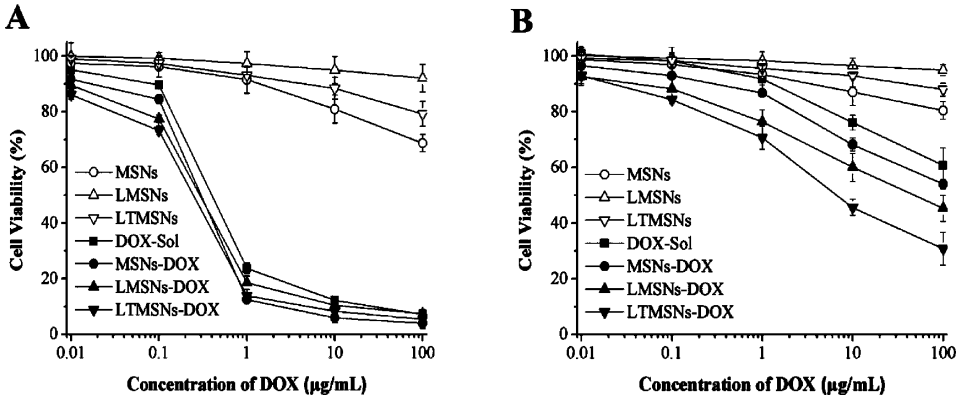

Figure 11. Cytotoxicity of various DOX formulations at serial DOX concentrations and the corresponding amount of blank nanocarriers against MCF-7 (A) and MCF-7/Adr (B) cells at 48 h.

DOI: 10.1021/am5082793
ACS Appl. Mater. Interfaces 2015, 7, 3342−3351

cells at high level ascribed to the low expression of P-gp, thus resulting in the equally high cytotoxicity. The IC_{50} value of DOX in LTMSNs−DOX, LMSNs−DOX, and MSNs−DOX was 2.7-, 1.8-, and 1.9-fold lower than that of DOX−Sol. The cytotoxicity assay of corresponding amount of blank nanocarriers contained in different formulations at serial DOX concentrations was also shown in Figure 11. The cell viability of two cell lines treated with MSNs was lower than that of LMSNs and LTMSNs, since the exposed silanol groups on MSNs can lead to the deformation of membrane lipids[36] and proteins when incubating with the cells, while after the lipid layer capping, the cytotoxicity greatly reduced due to the concealing of silanol groups. And the cell viability of LMSNs remained greater than 95% even at the highest test concentrations, indicating that the lipid layer capping could improve the biocompatibility of MSNs to some degree. As for LTMSNs, because of the presence of TPGS, which also had the antitumor effect (Supporting Information), a declining trend in cell viability could be observed with increasing concentration.

4. CONCLUSION

The prepared LTMSNs possessed various attractive features including comparably high LE%, redox-responsive controlled drug release, enhanced dispersing stability, and cellular internalization together with inhibition of P-gp-mediated efflux. As a result, the DOX within LTMSNs could be selectively delivered and intensively released in the cytoplasm of cancerous cells without premature leakage during circulation, thereby reducing the systemic toxicity. And it could also significantly improve the cytotoxicity of DOX against the cells with MDR by elevating the accumulation of drug in cells and retaining the drug concentration at a high level. In summary, the LTMSNs could be a promising vehicle for drug delivery to realize controlled drug release and overcome the MDR.

■ ASSOCIATED CONTENT

Supporting Information

The size distribution of LTMSNs in water, PBS, and saline containing 5% BSA as well as the cytotoxicity assay of corresponding amount of TPGS contained in DOX−LTMSNs formulations at serial DOX concentrations. This material is available free of charge via the Internet at http://pubs.acs.org.

■ AUTHOR INFORMATION

Corresponding Author

*Phone/Fax: +86 24 23986348. E-mail: silingwang@syphu.edu.cn.

Notes

The authors declare no competing financial interest.

■ ACKNOWLEDGMENTS

This work was supported by National Basic Research Program of China (973 Program, Grant No. 2015CB932100) and the National Natural Science Foundation of China (Grant No. 81473165).

■ REFERENCES

(1) Gottesman, M. M.; Fojo, T.; Bates, S. E. Multidrug Resistance in Cancer: Role of ATP−dependent Transporters. *Nat. Rev. Cancer* **2002**, *2*, 48−58.

(2) Stein, W.; Bates, S.; Fojo, T. Intractable Cancers: The Many Faces of Multidrug Resistance and The Many Targets It Presents for Therapeutic Attack. *Curr. Drug Targets* **2004**, *5*, 333−346.

(3) Gillet, J.-P.; Gottesman, M. M. Mechanisms of Multidrug Resistance in Cancer. In *Multi-Drug Resistance in Cancer;* Zhou, J., Ed.; Humana Press: New York, 2010; pp 47−76.

(4) Chaudhary, P. M.; Roninson, I. B. Expression and Activity of P-glycoprotein, a Multidrug Efflux Pump, in Human Hematopoietic Stem Cells. *Cell* **1991**, *66*, 85−94.

(5) Dong, X.; Mattingly, C. A.; Tseng, M. T.; Cho, M. J.; Liu, Y.; Adams, V. R.; Mumper, R. J. Doxorubicin and Paclitaxel-loaded Lipid-based Nanoparticles Overcome Multidrug Resistance by Inhibiting P-glycoprotein and Depleting ATP. *Cancer Res.* **2009**, *69*, 3918−3926.

(6) Deng, Z.; Yan, F.; Jin, Q.; Li, F.; Wu, J.; Liu, X.; Zheng, H. Reversal of Multidrug Resistance Phenotype in Human Breast Cancer Cells Using Doxorubicin-liposome−microbubble Complexes Assisted by Ultrasound. *J. Controlled Release* **2014**, *174*, 109−116.

(7) Yin, Q.; Shen, J.; Zhang, Z.; Yu, H.; Li, Y. Reversal of Multidrug Resistance by Stimuli-responsive Drug Delivery Systems for Therapy of Tumor. *Adv. Drug Delivery Rev.* **2013**, *65*, 1699−1715.

(8) Tang, F.; Li, L.; Chen, D. Mesoporous Silica Nanoparticles: Synthesis, Biocompatibility and Drug Delivery. *Adv. Mater.* **2012**, *24*, 1504−1534.

(9) Zhang, Y.; Zhi, Z.; Jiang, T.; Zhang, J.; Wang, Z.; Wang, S. Spherical Mesoporous Silica Nanoparticles for Loading and Release of the Poorly Water-soluble Drug Telmisartan. *J. Controlled Release* **2010**, *145*, 257−263.

(10) Lai, C.-Y.; Trewyn, B. G.; Jeftinija, D. M.; Jeftinija, K.; Xu, S.; Jeftinija, S.; Lin, V. S.-Y. A Mesoporous Silica Nanosphere-based Carrier System with Chemically Removable CdS Nanoparticle Caps for Stimuli-responsive Controlled Release of Neurotransmitters and Drug Molecules. *J. Am. Chem. Soc.* **2003**, *125*, 4451−4459.

(11) Gan, Q.; Lu, X.; Yuan, Y.; Qian, J.; Zhou, H.; Lu, X.; Shi, J.; Liu, C. A Magnetic, Reversible pH-responsive Nanogated Ensemble Based on Fe_3O_4 Nanoparticles-capped Mesoporous Silica. *Biomaterials* **2011**, *32*, 1932−1942.

(12) Park, C.; Kim, H.; Kim, S.; Kim, C. Enzyme Responsive Nanocontainers with Cyclodextrin Gatekeepers and Synergistic Effects in Release of Guests. *J. Am. Chem. Soc.* **2009**, *131*, 16614−16615.

(13) Chang, B.; Chen, D.; Wang, Y.; Chen, Y.; Jiao, Y.; Sha, X.; Yang, W. Bioresponsive Controlled Drug Release Based on Mesoporous Silica Nanoparticles Coated with Reductively Sheddable Polymer Shell. *Chem. Mater.* **2013**, *25*, 574−585.

(14) Xue, M.; Findenegg, G. H. Lysozyme as a pH-responsive Valve for the Controlled Release of Guest Molecules from Mesoporous Silica. *Langmuir* **2012**, *28*, 17578−17584.

(15) Wang, J. L.; Sun, J.; Chen, Q.; Gao, Y.; Li, L.; Li, H.; Leng, D. L.; Wang, Y. J.; Sun, Y. H.; Jing, Y. K.; Wang, S. L.; He, Z. G. Star-shape Copolymer of Lysine-linked Di-tocopherol Polyethylene Glycol 2000 Succinate for Doxorubicin Delivery with Reversal of Multidrug Resistance. *Biomaterial* **2012**, *33*, 6877−6888.

(16) Cheng, R.; Feng, F.; Meng, F. H.; Deng, C.; Feijen, J.; Zhong, Z. Y. Glutathione-responsive Nano-vehicles as a Promising Platform for Targeted Intracellular Drug and Gene Delivery. *J. Controlled Release* **2011**, *152*, 2−12.

(17) Saito, G.; Swanson, J. A.; Lee, K. D. Drug Delivery Strategy Utilizing Conjugation via Reversible Disulfide Linkages: Role and Site of Cellular Reducing Activities. *Adv. Drug Delivery Rev.* **2003**, *55*, 199−215.

(18) Ashley, C. E.; Carnes, E. C.; Phillips, G. K.; Padilla, D.; Durfee, P. N.; Brown, P. A.; Hanna, T. N.; Liu, J.; Phillips, B.; Carter, M. B. The Targeted Delivery of Multicomponent Cargos to Cancer Cells by Nanoporous Particle-supported Lipid Bilayers. *Nat. Mater.* **2011**, *10*, 389−397.

(19) Wang, L. S.; Wu, L. C.; Lu, S. Y.; Chang, L. L.; Teng, I.-T.; Yang, C.-M.; Ho, J. A. Biofunctionalized Phospholipid-capped Mesoporous Silica Nanoshuttles for Targeted Drug Delivery: Improved Water Suspensibility and Decreased Nonspecific Protein Binding. *ACS Nano* **2010**, *4*, 4371−4379.

(20) Teng, I.; Chang, Y. J.; Wang, L. S.; Lu, H. Y.; Wu, L. C.; Yang, C. M.; Chiu, C. C.; Yang, C. H.; Hsu, S. L.; Ho, J. A. Phospholipid-

DOI: 10.1021/am5082793
ACS Appl. Mater. Interfaces 2015, 7, 3342−3351

functionalized Mesoporous Silica Nanocarriers for Selective Photodynamic Therapy of Cancer. *Biomaterials* **2013**, *34*, 7462−7470.
(21) van Schooneveld, M. M.; Vucic, E.; Koole, R.; Zhou, Y.; Stocks, J.; Cormode, D. P.; Tang, C. Y.; Gordon, R. E.; Nicolay, K.; Meijerink, A. Improved Biocompatibility and Pharmacokinetics of Silica Nanoparticles by Means of a Lipid Coating: A Multimodality Investigation. *Nano Lett.* **2008**, *8*, 2517−2525.
(22) Collnot, E. M.; Baldes, C.; Wempe, M. F.; Kappl, R.; Hüttermann, J.; Hyatt, J. A.; Edgar, K. J.; Schaefer, U. F.; Lehr, C. M. Mechanism of Inhibition of P-glycoprotein Mediated Efflux by Vitamin E TPGS: Influence on ATPase Activity and Membrane Fluidity. *Mol. Pharmaceutics* **2007**, *4*, 465−474.
(23) Youk, H. J.; Lee, E.; Choi, M. K.; Lee, Y. J.; Chung, J. H.; Kim, S. H.; Lee, C. H.; Lim, S. J. Enhanced Anticancer Efficacy of α-Tocopheryl Succinate by Conjugation with Polyethylene Glycol. *J. Controlled Release* **2005**, *107*, 43−52.
(24) Tewey, K. M.; Chen, G.; Nelson, E.; Liu, L. Intercalative Antitumor Drugs Interfere with the Breakage-reunion Reaction of Mammalian DNA Topoisomerase II. *J. Bio. Chem.* **1984**, *259*, 9182−9187.
(25) Arola, O. J.; Saraste, A.; Pulkki, K.; Kallajoki, M.; Parvinen, M.; Voipio-Pulkki, L. M. Acute Doxorubicin Cardiotoxicity Involves Cardiomyocyte Apoptosis. *Cancer Res.* **2000**, *60*, 1789−1792.
(26) Emilienne Soma, C.; Dubernet, C.; Bentolila, D.; Benita, S.; Couvreur, P. Reversion of Multidrug Resistance by Co-encapsulation of Doxorubicin and Cyclosporin A in Polyalkylcyanoacrylate Nanoparticles. *Biomaterials* **2000**, *21*, 1−7.
(27) Möller, K.; Kobler, J.; Bein, T. Colloidal Suspensions of Nanometer-sized Mesoporous Silica. *Adv. Funct. Mater.* **2007**, *17*, 605−612.
(28) He, C. B.; Hu, Y. P.; Yin, L. C.; Tang, C.; Yin, C. H. Effects of Particle Size and Surface Charge on Cellular Uptake and Biodistribution of Polymeric Nanoparticles. *Biomaterials* **2010**, *31*, 3657−3666.
(29) Kecht, J.; Schlossbauer, A.; Bein, T. Selective Functionalization of the Outer and Inner Surfaces in Mesoporous Silica Nanoparticles. *Chem. Mater.* **2008**, *20*, 7207−7214.
(30) Moghimi, S. M.; Hunter, A. C.; Murray, J. C. Nanomedicine: Current Status and Future Prospects. *FASEB J.* **2005**, *19*, 311−330.
(31) Muthu, M. S.; Kulkarni, S. A.; Raju, A.; Feng, S.-S. Theranostic Liposomes of TPGS Coating for Targeted Co-delivery of Docetaxel and Quantum Dots. *Biomaterials* **2012**, *33*, 3494−3501.
(32) Chang, B.; Guo, J.; Liu, C.; Qian, J.; Yang, W. Surface Functionalization of Magnetic Mesoporous Silica Nanoparticles for Controlled Drug Release. *J. Mater. Chem.* **2010**, *20*, 9941−9947.
(33) Zhu, Y.; Ikoma, T.; Hanagata, N.; Kaskel, S. Rattle-Type Fe_3O_4@SiO_2 Hollow Mesoporous Spheres as Carriers for Drug Delivery. *Small* **2010**, *6*, 471−478.
(34) Zhang, X.; Li, F.; Guo, S.; Chen, X.; Wang, X.; Li, J.; Gan, Y. Biofunctionalized Polymer-lipid Supported Mesoporous Silica Nanoparticles for Release of Chemotherapeutics in Multidrug Resistant Cancer Cells. *Biomaterials* **2014**, *35*, 3650−3665.
(35) Hatakeyama, H.; Akita, H.; Harashima, H. A Multifunctional Envelope Type Nano Device (MEND) for Gene Delivery to Tumours Based on the EPR Effect: A Strategy for Overcoming the PEG Dilemma. *Adv. Drug Delivery Rev.* **2011**, *63*, 152−160.
(36) Tao, Z.; Toms, B. B.; Goodisman, J.; Asefa, T. Mesoporosity and Functional Group Dependent Endocytosis and Cytotoxicity of Silica Nanomaterials. *Chem. Res. Toxicol.* **2009**, *22*, 1869−1880.

DOI: 10.1021/am5082793
ACS Appl. Mater. Interfaces 2015, 7, 3342−3351